Journal of Marine Science and Technology

Volume 26 | Issue 1 Article 10

CHLOROPHYLL CONCENTRATION DERIVED FROM MICROWAVE REMOTE SENSING MEASUREMENTS USING ARTIFICIAL NEURAL NETWORK ALGORITHM

Young-Heon Jo
Department of Oceanography, Pusan National University, Busan, 46241, Republic of Korea., joyoung@pusan.ac.kr

Dae-Won Kim
Department of Oceanography, Pusan National University, Busan, 46241, Republic of Korea.

Hyuna Kim
Department of Oceanography, Pusan National University, Busan, 46241, Republic of Korea.

CHLOROPHYLL CONCENTRATION DERIVED FROM MICROWAVE REMOTE SENSING MEASUREMENTS USING ARTIFICIAL NEURAL NETWORK ALGORITHM

Acknowledgements

This research was supported by the National Research Foun- dation of Korea (NRF) grant funded by the Korean government(MSIP) (NRF-2014R1A2A1A11051742) and by the “Development of the integrated data processing system for GOCI-II” funded by the Ministry of Oceans and Fisheries, Korea.

Journal of Marine Science and Technology, Vol. 26, No. 1, pp. 102-110 (2018)
DOI: 10.6119/JMST.2018.02_(1).0004

CHLOROPHYLL CONCENTRATION DERIVED FROM MICROWAVE REMOTE SENSING MEASUREMENTS USING ARTIFICIAL NEURAL NETWORK ALGORITHM

Young-Heon Jo, Dae-Won Kim, and Hyuna Kim

Key words: neural network, ocean color, chlorophyll, cloud fill algorithm, GOCI.

ABSTRACT

Ocean color optic remote sensing has been used to estimate various biogeochemical constituents to monitor ocean environmental changes in coastal regions and global open oceans. However, the most problematic issue in utilizing ocean color measurements is cloud coverage. Thus, this study introduces a neural network (NN) algorithm to derive Chlorophyll a (Chl) concentrations, which are unavailable due to the presence of clouds. Because ocean color remote sensing depends on cloud coverage, microwave measurements, including sea-surface temperature, cloud, water vapor, precipitation, and winds, were used as inputs for the NN algorithm. Accordingly, the NN algorithm was designed to predict Chl using five inputs of microwave measurements and geolocation data. The correlation coefficient and root mean square error between the predicted and remotely sensed Chl concentrations were about 0.89 and 0.30 mg/m^3, respectively. Therefore, the developed NN algorithm enabled us to obtain Chl concentration during cloudy days, and even typhoon passages, as demonstrated in this study. However, Chl concentrations along coastal regions could not be predicted based on the inputs of the NN algorithm. Microwave remote sensing could not measure inhomogeneous emissivity for areas that were partially ocean and land, such as near-coastal regions.

I. INTRODUCTION

Remotely sensed ocean color measurements taken by various satellites help scientists better understand changes in phytoplankton and how these changes affect the Earth system. These small organisms can not only affect very small-scale systems but can also lead to large-scale climate changes. Thus, understanding and monitoring phytoplankton through Chlorophyll a (Chl) measurements can help scientists study and predict environmental changes. However, ocean color measurements are limited by weather conditions, especially clouds. Because these measurements rely on optical sensors, there are no ways to take measurements if clouds are present. Fig. 1 shows days of cloud coverage based on the Moderate Resolution Imaging Spectroradiometer (MODIS) sensor on NASA's Aqua satellite. Although the coastal regions are generally less cloudy than warm open oceans, most regions have cloud cover on more than 250 days per year, and thus, no Chl measurements are available for these regions. Accordingly, an important task to obtain Chl data from remotely sensed spectral measurements is screening clouds. Efforts of discriminating clouds from various satellite measure-

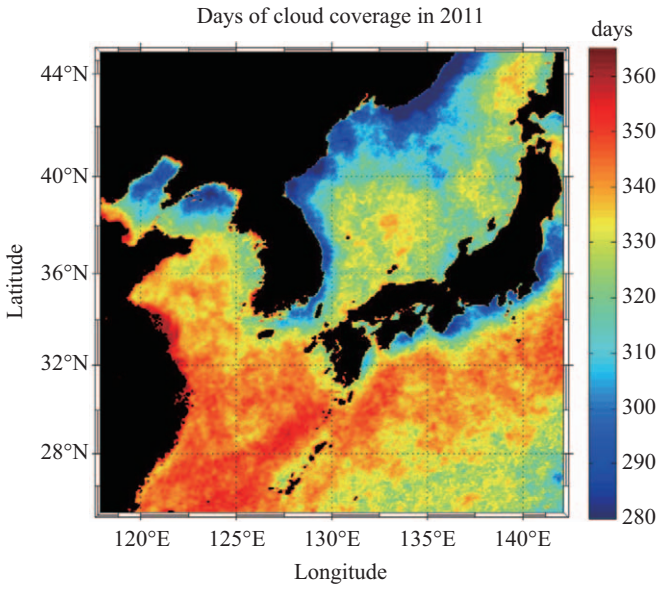

Fig. 1. Days of cloud covered regions estimated by Aqua-MODIS in 2011. Most of the regions have more than 300 days of cloud coverage in a year.

Paper submitted 10/12/16; revised 03/29/17; accepted 07/25/17. *Author for correspondence: Young-Heon Jo (e-mail: joyoung@pusan.ac.kr).*
Department of Oceanography, Pusan National University, Busan, 46241, Republic of Korea.

ments can be found in the literature (Ackerman et al., 1998; Liu et al., 2004; Li et al., 2005; Liu et al., 2014; Wang et al., 2014).

There are different methods for interpolating data or filling missing coverage due to clouds, ranging from simple linear interpolation and bicubic splines to the use of complicated statistical methods. For instance, a univariate approach has been used to reconstruct missing data by considering only information on a specific variable to infer values at missing data locations (Beckers and Rixen, 2003; Kondrashov and Ghil, 2006). However, oceanographic phenomena are interrelated by ocean dynamics, making it potentially useful to utilize these relations when reconstructing missing data. In addition to using a univariate approach, the Data INterpolating Empirical Orthogonal Functions (DINEOF) method has been used to analyze variables with the help of related multiple measurements (e.g., Alvera-Azcárate et al., 2005; Sirjacobs et al., 2011). The DINEOF method uses input imagery, which is condensed in a two-dimensional matrix for temporal and spatial components. The basic idea of the DINEOF method is to fill the missing data by proceeding iterative cycles of singular value decompositions (SVDs) to produce a set of empirical orthogonal functions (EOFs).

Another potential method utilizes a neural network (NN) approach, which is widely used as a continuous model to fit nonlinear transfer functions. Several studies based on ocean color measurements have shown that NN techniques can derive water constituents in both Case I and Case II waters (Buckton et al., 1999; Schiller and Doerffer, 1999; Gross et al., 2000). Although Case I waters represent the phytoplankton-dominant cases, Case II waters represent all other possible cases (especially particulate matter or yellow substances). Specifically, Case I waters can range from oligotrophic to eutrophic conditions. In Case II waters, substances are not linked to Chl concentration, but instead must be treated as independent variables (IOCCG, 2000). Algorithms based on NN techniques are less sensitive to noise than empirical methods. Thus, NN techniques are a promising method for deriving oceanic constituents from ocean color data. For instance, Gross et al. (1999) used an NN technique to retrieve chlorophyll pigments in the near surface from ocean color measurements based on bio-optical inversion, which is established by analyzing concomitant sunlight spectral reflectance over the ocean surface and pigment concentration. Gross et al. (1999) showed the advantages of neural function approximation, such as the association of nonlinear complexity and noise filtering. Zhang et al. (2003) reported a method to retrieve pigment concentration in Case I waters from ocean color. The method is derived from radiative transfer (RT) simulations and subsequent application of artificial NN techniques.

Although NN methods have been employed for ocean color research to better estimate ocean color products, they have not been specifically used to fill gaps in ocean color measurements due to clouds. In this study, we applied NN methods to microwave remote sensing measurements to fill the gaps in MODIS measurements. Accordingly, we could obtain continuous Chl concentrations under different weather conditions, such as heavy cloud coverage or hurricane passage. Thus, to fill gaps in observations, we discuss the feasibilities of whether this NN algorithm can be used to provide cloud-related missing ocean measurement data.

In this study, we applied an NN method, a feed-forward back propagation (FFBP) algorithm, to fill missing Chl resulting from the presence of clouds around the Korean Peninsula. We contended that the FFBP algorithm was advantageous in predicting cloud fill Chl values from one-dimensional individual random ground truth measurements, and that it enabled us to obtain a cloud-free map using two-dimensional microwave satellite measurements. The rest of this paper is organized as follows. We describe the data and methodology for the NN method in Section 2, and analyze the two results—performance of NN and two cases for Chl prediction using NN—in Section 3. In Section 4, we discuss the findings and limitations of this study.

II. DATA AND METHOD

1. Ocean Color Data

The primary source of satellite Chl data for this study is MODIS (http://oceancolor.gsfc.nasa.gov/ftp.html), which detects a wide range of electromagnetic energy and takes measurements at three spatial resolutions. We use the daily mean of MODIS Chl in 4 km spatial resolutions for the Chl concentration from January 2011 to December 2012. Because we intend to compare the predicted Chl based on NN, we also use the Geostationary Ocean Color Imager (GOCI) data, which are available from April 2011 to the present.

GOCI is the first geostationary ocean color satellite sensor, which has an advantage over other ocean color sensors in that it collects eight measurements per day during the daytime, enabling the monitoring of temporal variability of the ocean environment. The spatial coverage of GOCI is a 2500 km × 2500 km area around the Korean Peninsula centered at 36°N, 130°E, consisting of 16(4 × 4) slot images. We use GOCI level 2 Chl data with a spatial resolution of 500 m × 500 m.

2. Microwave Data

We obtain microwave data from the AMSR instruments (http://www.remss.com/missions/amsre). In order to match up the daily observations, we map AMSR data to a 0.25° grid divided into two maps based on ascending and descending passes. The data are in the following order: time (UTC), sea-surface temperature (SST), low-frequency 10-m surface wind speed (WSPD-LF), medium-frequency 10-m surface wind speed (WSPD-MF), atmospheric water vapor (VAPOR), cloud liquid water (CLOUD), and rain rate (RAIN), followed by seven night-time maps in the same order.

3. NN Algorithm

A feedforward NN design involves a series of interconnected nodes and neurons that are divided into input, hidden, and output layers (Fig. 2). The input layer receives microwave measurements and geolocation information and passes them to the hidden layer, which is a system of layered nodes that has many

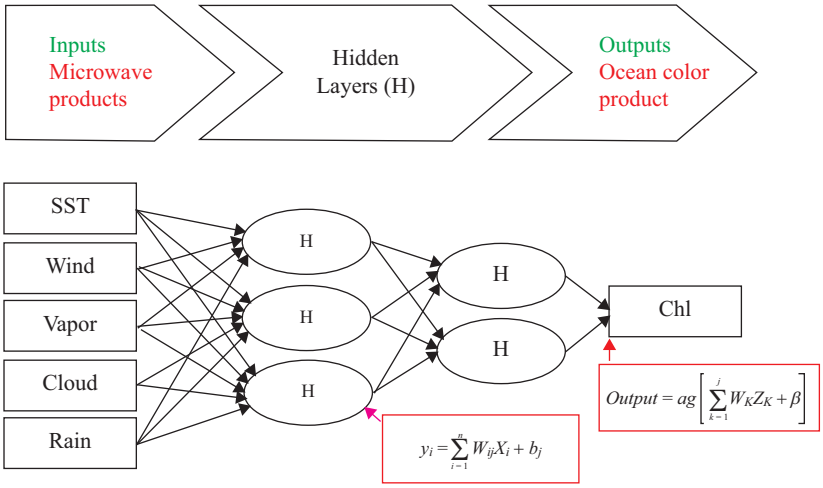

Fig. 2. A schematic diagram for the neural network for this study. Five inputs of microwave measurements and geolocation (not shown), two hidden layers (H) and one output such as Chl for this study.

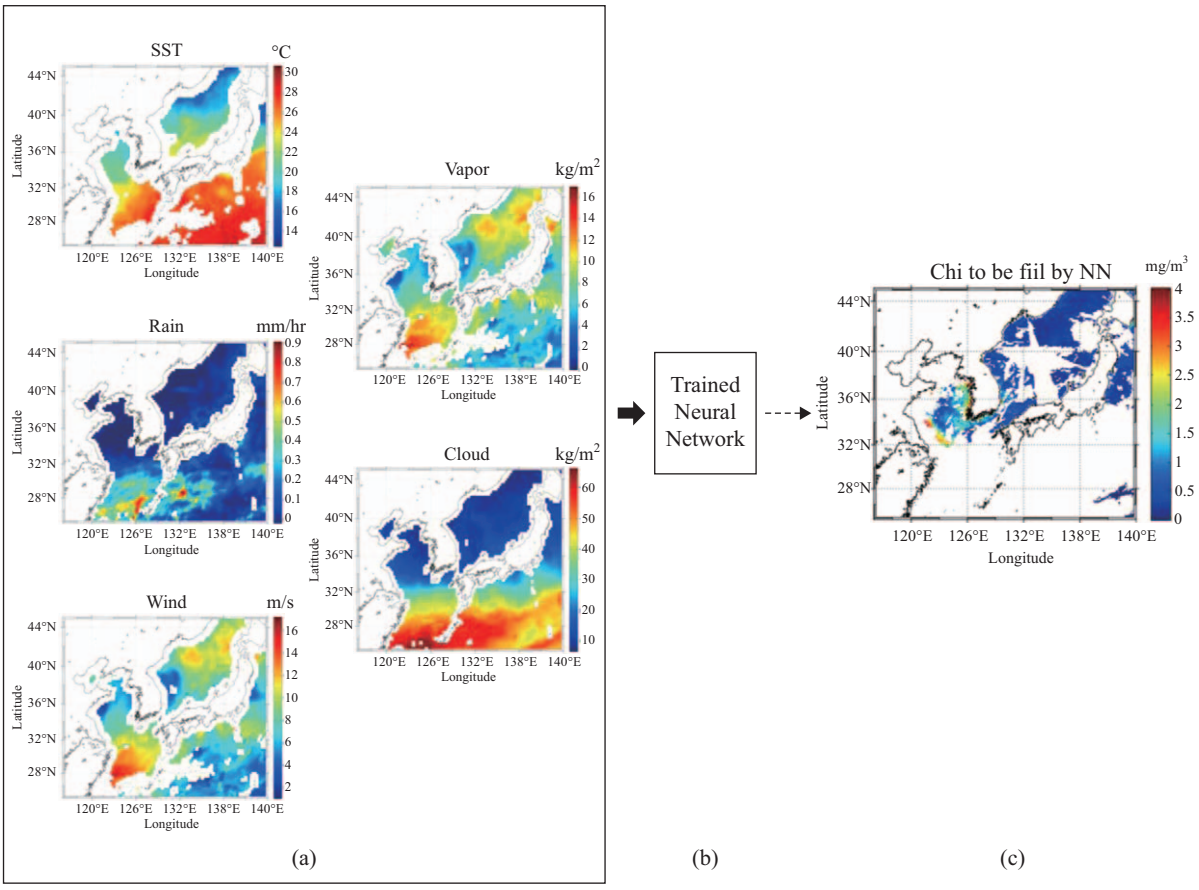

Fig. 3. As an example, five microwave measurements (a) in April 10, 2011 which were used to be simulated by trained neural network (b) to predict Chl. The Chl (c) will be predicted by well-trained neural network.

neurons in each layer. These neurons consist of a linear summation function and a nonlinear activation function, enabling the network to process data as illustrated in Fig. 3. The sensitivity for different combinations of inputs is discussed in the Discussion section.

We design three NN processes in this study to split the available data into three datasets: a training dataset (70% of the data), a validation dataset (15%), and a test dataset (15%). The training dataset is used to adjust the weights on the NN and the validation dataset is used to minimize overfitting during the training

process. During the validation process, we do not adjust the weights of the network, but verify any increase in accuracy over the training dataset. If the accuracy over the training dataset increases, but the accuracy over the validation dataset does not, then we are overfitting our NN and stop training. Once training and validation have been completed, the testing dataset is used only for the final solution to confirm the predictive power of the network for Chl.

The inputs to each neuron are first routed to the summation function defined below (Keiner and Yan, 1998; Dzwonkowski and Yan, 2005; Jo et al., 2012):

$$y_i = \sum_{i=1}^{n} W_{ij} X_i + b_j \,, \tag{1}$$

where W_{ij} is the weight associated with each input/node connection, X_i is the input, and b_j is the bias associated with node j, which is the number of neurons in the hidden layer. The output, y_i, is mapped to a value between (-1, 1). After the initial data pass through the neurons of the hidden and output layers, a value for the desired geophysical parameter is produced as shown in Eq. (2).

$$Output = ag\left[\sum_{k=1}^{j} W_K \, Z_k + \beta\right], \tag{2}$$

where a is a scaling factor, g[ ] is the nonlinear activation function, W_k and Z_k are the weights and inputs between the neuron layers, β is the bias associated with the output layer, and j is the number of neurons in the hidden layer. This output is then compared with the target data from which the network error is determined. The error is then backpropagated through the network to adjust the weights and biases associated with each neuron in the network layers. The repeated forward feed of the network inputs, in conjunction with the backpropagation, progressively minimizes the network error.

As Fig. 3 shows, the five microwave measurements (Fig. 3(a)) cover most regions except the coastal regions. These measurements with geolocations (longitude and latitude) are used to train, validate, and test Chl in the NN processes (Fig. 3(b)). Thus, the missing Chl information in Fig. 3(c) will be filled with predicted Chl.

III. RESULTS

1. NN Performance

It remains difficult to reliably fill gaps in ocean color data for the global oceans, primarily due to cloud coverage. However, if we incorporate certain parameters changing Chl in the NN processes, we can predict Chl for even cloud-covered regions. Thus, in order to justify why the five inputs (SST, winds, cloud, vapor, and precipitation) are used for the NN processes, we introduce several studies as follows. According to Eppley (1972), the maximum expected increasing rate of Chl can be estimated from SST, and thus, the maximum expected assimilation number (i.e., rate of photosynthetic carbon assimilation per weight of Chl) can also be estimated. Thus, SST directly contributes to changes in Chl. For instance, the correlation between SST and Chl of phytoplankton in the Black Sea was approximately 0.6 with a significance at $p < 0.05$ (Kavak and Karadogan, 2012). However, winds contribute indirectly to changes in Chl through wind-driven upwelling or downwelling (e.g., Kim et al., 2007), which is a well-known phenomenon. For instance, the relation between wind and bloom initiation based on remotely sensed wind stress data and ocean color data shows that in spring, blooms began 6-15° days after wind stress weakened and that fall blooms started 3-9 days after winds strengthened. Although the results of these previous studies are based on monthly observations, the daily microwave measurements to predict Chl using NN are still applicable, because Chl concentrations are influenced by the changes of SST, wind, cloud cover, vapor, and precipitation simultaneously and gradually.

Cloud and Chl changes have an indirect relation through the fraction of solar radiation that penetrates the sea and is absorbed by plants during photosynthesis. This energy is used in the conversion of inorganic matter to organic compounds (Lalli and Parsons, 1997). The amount of radiation reaching the sea surface at any point is thus a function of sun angle, the length of the day, and weather conditions. According to Kim et al. (2014), precipitation over the ocean surface can increase ocean nitrate concentration, and consequently, enhance Chl (a proxy for phytoplankton biomass). The study also showed that an increase in wind speed accompanied by precipitation events was a major contributor to the Chl changes observed during wet days, whereas the wet deposition of pollutant nitrogen slightly increased Chl concentration (< 5%) only in nutrient-depleted areas. Therefore, the inputs we used are directly or indirectly related to Chl in response to precipitation events.

Fig. 3(a) shows how the NN algorithm processes the five input data sources (microwave measurements) plus two geolocations (longitude and latitude; not shown). To fill the gaps of Chl data measured by MODIS (Fig. 4(a)), the NN takes three processes: training (red), validation (black), and prediction (green) (Fig. 4(b)). MODIS Chl (black) is used to estimate correlation and root mean square error (RMSE) with three NN-predicted Chl values. The correlation coefficients and RMSE for training, validation, and prediction are 0.9 and 0.25 mg/m^3, 0.89 and 0.12 mg/m^3, and 0.89 and 0.30 mg/m^3, respectively. The results are determined when the correlation coefficient is higher and RMSE is lower during the training processes. For the hidden layer in this process (Fig. 2), we use 40 nodes for the first layer and 30 nodes for the second layer, which produce the best results.

Note that the NN estimations (Fig. 4(b)) are underestimated compared to the MODIS Chl measurements, resulting from the normalized NN processes. After applying a well-trained NN, Chl is predicted for January 1, 2011 (Fig. 4(c)), and the original MODIS Chl and predicted Chl are incorporated as shown in Fig. 4(d). The significant differences between Figs. 4(a) and 4(c)

Table 1. Correlation coefficients and RMSE for the different inputs.

NN inputs	Train Correlation/RMSE	Validate Correlation/RMSE	Test Correlation/RMSE
Rain, wind, vapor	0.8/0.36	0.79/0.16	0.79/0.42
Rain, SST, vapor	0.82/0.33	0.83/0.16	0.82/0.39
Rain, SST, wind	0.82/0.32	0.82/0.15	0.82/0.39
SST, wind, vapor	0.82/0.33	0.81/0.16	0.82/0.40
Cloud, rain, SST	0.82/0.33	0.82/0.16	0.82/0.39
Cloud, rain,vapor	0.83,0.32	0.82/0.16	0.83/0.38
Cloud, rain, wind	0.81/0.33	0.81/0.15	0.81/0.40
Cloud, SST, vapour	0.83/0.32	0.83/0.14	0.83/0.38
Cloud, SST, wind	0.81/0.34	0.81/0.15	0.81/0.40
Cloud, rain, SST, vapor	0.83/0.32	0.83/0.16	0.83/0.38
Cloud, wind, vapor	0.83/0.32	0.84/0.14	0.83/0.38
Cloud, rain, SST, wind	0.80/0.35	0.80/0.16	0.80/0.41
Cloud, rain, wind, vapor	0.80/0.34	0.80/0.16	0.80/0.41
Cloud, SST, wind, vapor	0.82/0.33	0.83/0.14	0.82/0.39
Rain, SST, wind, vapor	0.80/0.34	0.80/0.15	0.80/0.41
Cloud, SST, wind, vapour, rain	0.90/0.25	0.89/0.12	0.89/0.30

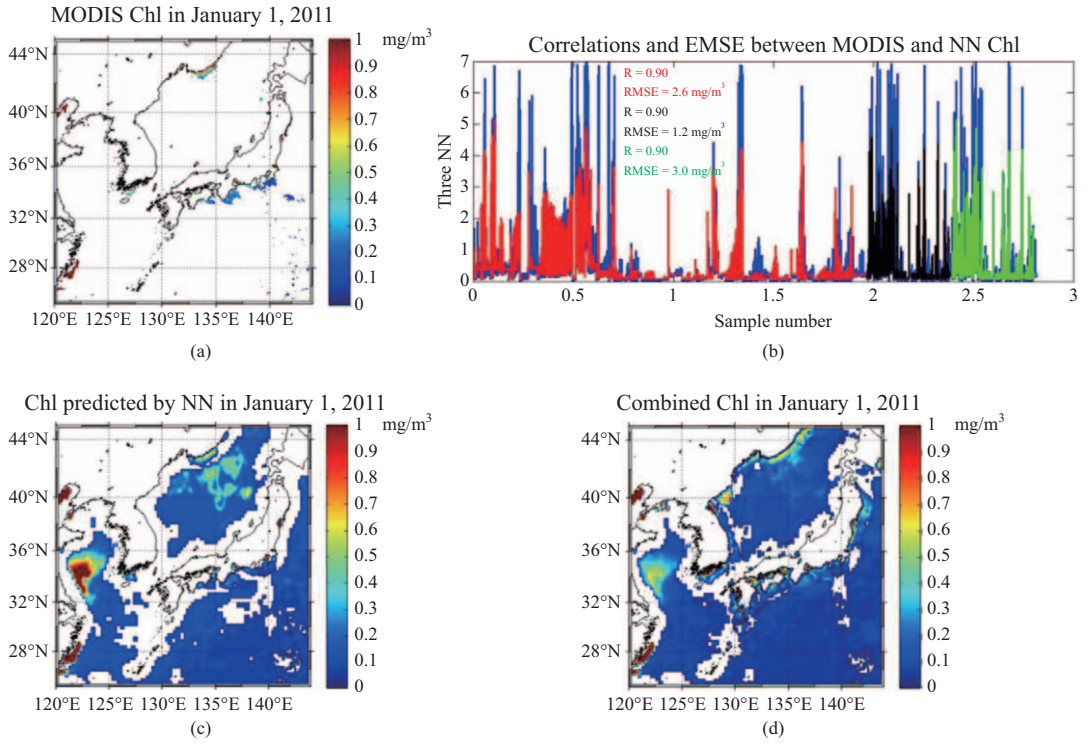

Fig. 4. Chl in January 1, 2011(a) was reproduced by neural network (b) as shown in (c). Then original Chl observations (a) and predicted Chl (c) were merged as shown in (d). The three process to obtain well-trained neural network are shown with correlations and RMSE in Fig. 4(b). The blue, red, black and green lines show the original data, trained NN, validated NN, and tested NN data, respectively.

are Chl information; Chl measured by MODIS is almost missed, but the NN-predicted Chl is filled. Chl is not available in the central East Japan Sea, and the predicted Chl in Fig. 4(c) shows fully covered Chl variability as the microwave measurements as inputs cannot resolve coastal regions unlike optical remote sensing sensors such as MODIS. Combining the original MODIS Chl and NN-predicted Chl, as shown in Fig. 4(d), allows us to obtain wide areas of Chl. The comparisons between NN-predicted Chl and GOCI Chl measurements are discussed in the following section.

We evaluate the sensitivity of different inputs (Table 1). The most sensitive inputs to predict Chl using different combinations

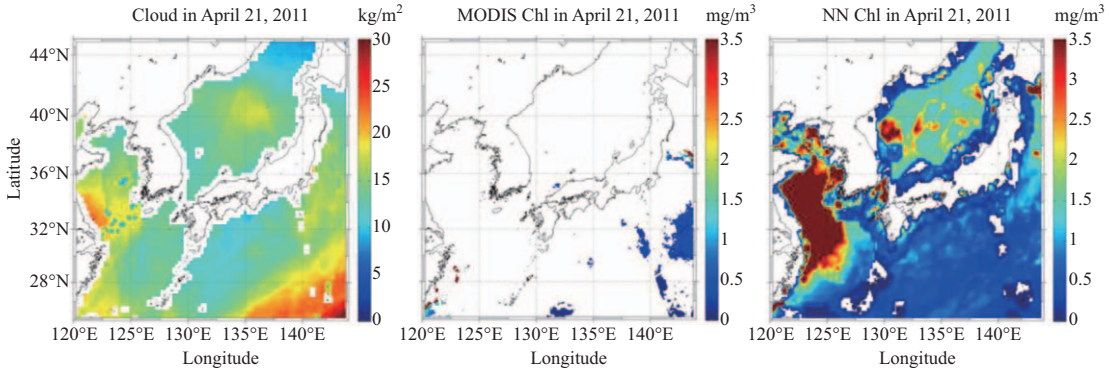

Fig. 5. The well-trained neural network was applied to a very cloudy day (a), and was not able to measure Chl as shown in Fig. 5(b), but the NN algorithm is able to fill the gaps as shown in Fig. 5(c). The RMSE between NN Chl (c) and MODIS Chl (b) is 0.7mg/m^3.

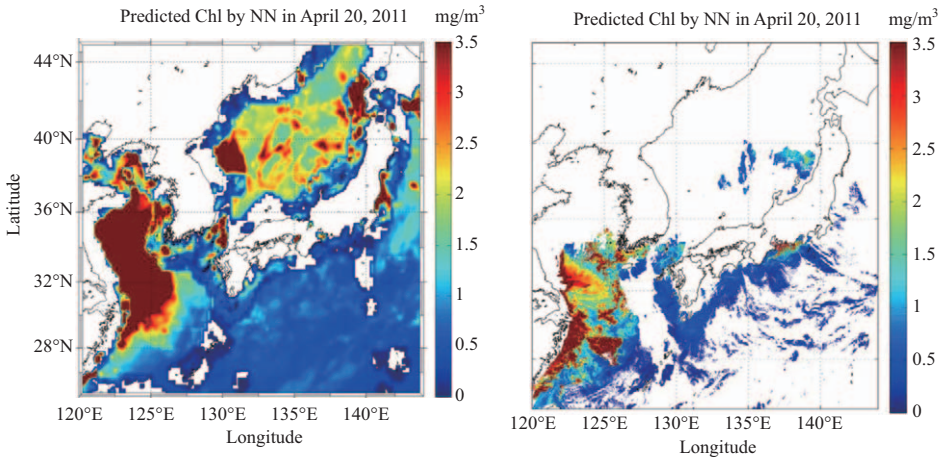

Fig. 6. Comparisons between predicted Chl by NN (a) and GOCI Chl (b) in April 20, 2011. The areas with gaps in Fig. 6(a) are due to the input microwave measurements, which do not cover near the coastal regions and islands.

of microwave measurements are SST and winds derived from AMSR. The Chl prediction with cloud, precipitation, and atmospheric vapor does not differ much from that without these combinations. The differences of the correlation coefficients and RMSE are an order less than 0.1 and 0.2 mg/m^3, respectively. This is not because there are no relations between them, but because there are not enough measurements at co-located regions (MODIS vs. AMSR microwave measurements). However, all inputs—SST, wind, vapor, clouds, and rain—for NN prediction perform better in terms of higher correlation coefficients and RMSE, respectively, as Table 1 shows.

2. Case 1: Deriving Chl in the Regions of Cloud and Atmospheric Vapor Contents

We apply the well-trained NN to inputs that were not used in the training and validation stages (Fig. 4(b)). Fig.5 shows an example of the cloud filling case under conditions of heavy cloud on April 21, 2011. Cloud information is derived from AMSR microwave measurements, leading to no Chl information available, as shown in Fig. 5(b). However, the NN algorithm with microwave measurements enables us to obtain continuous Chl information (Fig. 5(c)). One can compare Chl coverage in Figs. 5(b) and 5(c) on April 21, 2011. If the Chl prediction by the NN algorithm is not consistent, the Chl values in Fig. 5(c) will not be smoothly continued in different periods. In other words, if the Chl prediction processes by NN algorithm are not consistent, the Chl values will abruptly change day by day. We also examine days of high atmospheric water vapor content similar to that shown in Fig. 5. We obtain similar results (not shown), suggesting that Chl prediction by the NN algorithm is applicable to other weather conditions.

We compare the NN-predicted Chl with the daily averaged Chl measurements by GOCI (Fig. 6). The predicted Chl (Fig. 6(a)) shows relatively high Chl values in the Yellow Sea and the East China Sea (ECS). However, the GOCI Chl measurements provide no data for the northern Yellow Sea and almost none for the East Japan Sea. Note that Chl features in the Yellow Sea and ECS are slightly different because the predicted Chl has a 0.25° resolution, while GOCI Chl has a 1 km spatial resolution. Thus, one can see more detailed features in GOCI measurements near the mouth of the Yangtze River. Although NN-predicted Chl values are not comparable with GOCI with

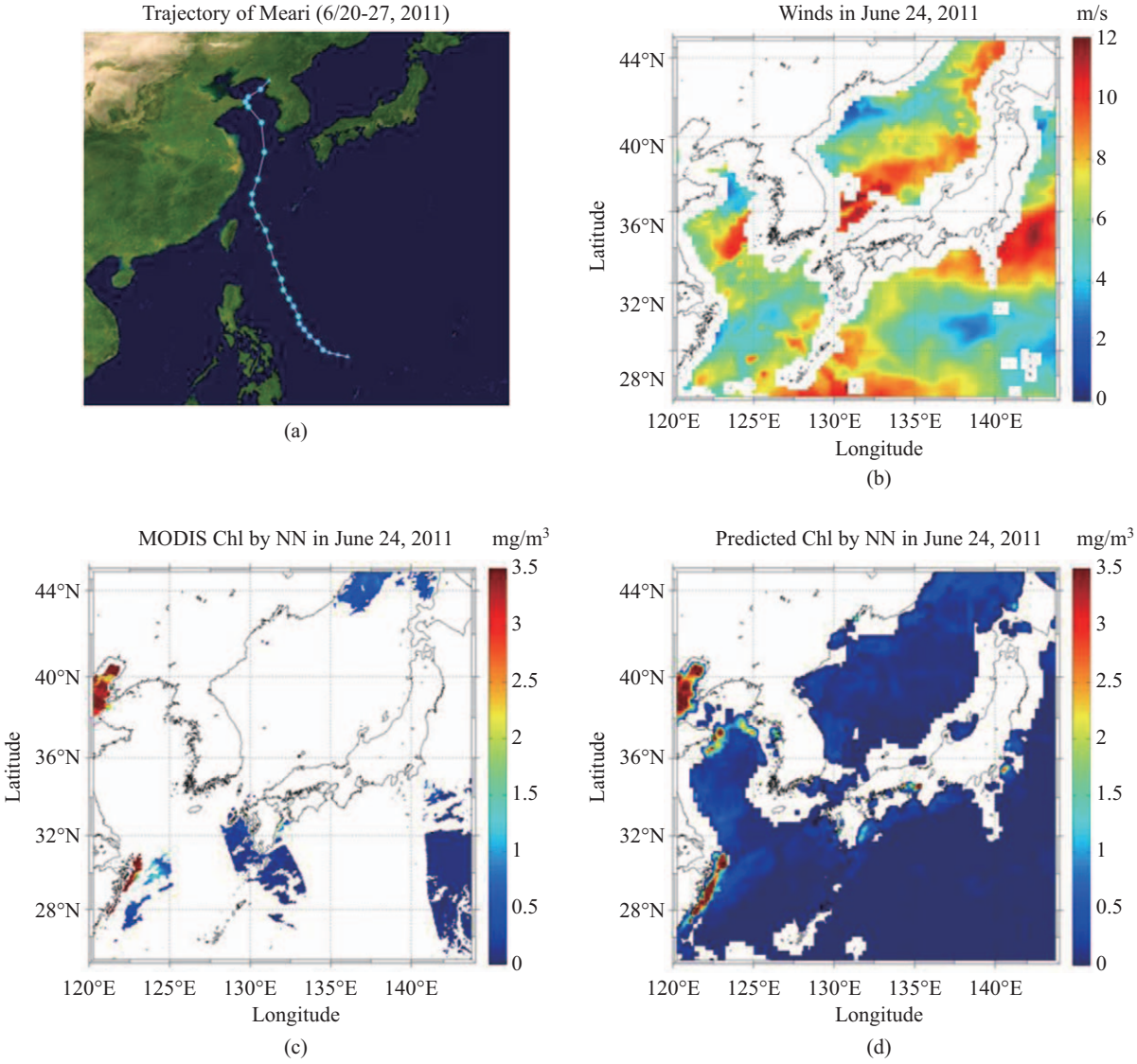

Fig. 7 The well-trained neural network was applied to obtain Chl during Typhoon Meari passage (a). The wind pattern as the one of five microwave inputs is shown in Fig. 7(b) and Chl is almost not available due to Typhoon (c). The predicted Chl by NN is shown in Fig. 7(d).

respect to spatial resolutions, Chl information is available for the study area. Note also that the differences between NN-predicted and GOCI Chl measurements (Fig. 6) are due to the following reason. Although the MODIS Chl is used for NN training, validation, and testing, GOCI Chl is used for simple comparisons. Although we use GOCI Chl for comparison, the Chl values derived from MODIS are not of the same magnitude (not shown) when compared to GOCI Chl due to different Chl algorithms and a slightly different atmospheric correction processes. However, the general spatial patterns between NN-based Chl and GOCI Chl are similar.

3. Case 2: Deriving Chl in the Regions of Typhoon Passage

The physical mechanism for the increase in Chl concentration after a typhoon passage is that a typhoon's strong wind induces mixing and upwelling in the upper ocean (Price, 1981), which brings subsurface Chl to the surface and subsurface nutrients into the euphotic zone (Babin et al., 2004; Zheng & Tang, 2007; Lin et al., 2008; Zheng et al., 2008; Zhao et al., 2008). The stronger the upwelling is, the more nutrients are brought to the surface. However, whether the typhoons have noticeable impacts on the ocean's primary production is still open for discussion.

To examine the influence of a typhoon passage, we estimate Chl using a well-trained NN and compare it with GOCI Chl measurements during Typhoon Meari. Previous research based on the impact of Meari in 2004 in the ECS was reported by Siswanto et al. (2008). They reported a three-fold primary production increase in ECS, which contributes to 3.8% of the annual new production. However, no study has detailed the ocean's physical response causing high phytoplankton enhancement, mainly because of limited ocean color measurement availability.

Fig. 7(a) shows the trajectory of Typhoon Meari from June 20

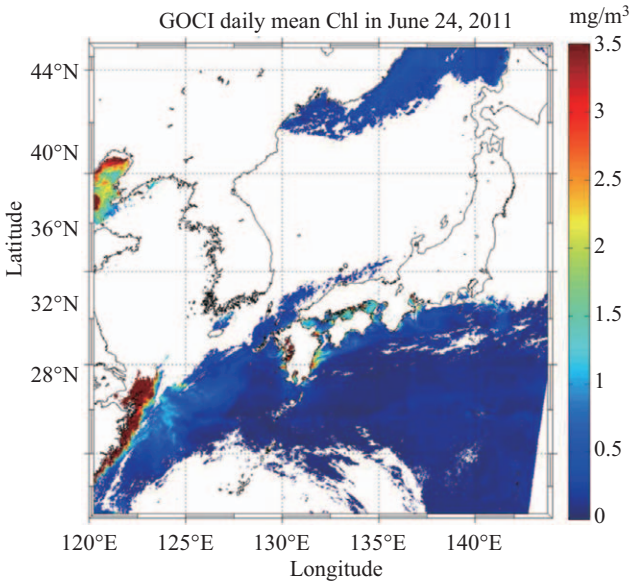

Fig. 8. Chl from GOCI measurements in June 24, 2011.

to 27, 2011. Fig. 7(b) is an example of the winds measured by ARMS-E on June 24, 2011. Because of the strong typhoon, MODIS Chl data on the same day are not available (Fig. 7(c)). Thus, we produce Chl using the NN algorithm as shown in Fig. 7(d). High Chl values can be found near the Yangtze River mouth and the Bohai Sea. We compare the NN-predicted Chl with Chl measured by GOCI on June 24, 2011 (Fig. 8). In general, the two Chl features are very similar (Figs. 7(d) and 8), but GOCI measurements reveal more detail due to their spatial resolution. Although Siswanto et al.'s study shows sub-mesoscale blooms along the typhoon track, the NN-predicted Chl cannot resolve it. Because the microwave remote sensing measurements are used for NN inputs, the NN-based Chl prediction cannot obtain sub-mesocale features due to coarse spatial resolutions.

IV. DISCUSSION AND CONCLUSION

The most problematic issue in utilizing ocean color measurements is cloud coverage. To overcome this problem, we apply a neural network algorithm, for the first time, to microwave satellite measurements, which are unaffected by weather conditions. Although the spatial resolution of the Chlorophyll concentration derived from microwave remote sensing measurements is coarse, this new approach has strong benefit for under bad weather conditions. Thus, this study develops an algorithm using an NN algorithm to fill gaps where Chl concentrations are unavailable due to cloud cover. The five microwave measurements include cloud, SST, precipitation, and winds.

Although the RMSE between tested NN and MODIS Chl measurements is 0.30 mg/m^3 (Fig. 4(b)), the RMSEs between predicted Chl by NN and MODIS and GOCI are larger due to the wide range of Chl values. Specifically, the RMSE values in Fig. 6 between NN-predicted Chl and MODIS Chl and between NN-predicted Chl and GOCI Chl are 1.9 and 1.23 mg/m^3, respectively. Furthermore, RMSEs in Figs. 7 and 8 are 0.7 mg/m^3 (between NN-predicted Chl and MODIS Chl) and 1.8 mg/m^3 (between NN-predicted Chl and GOCI Chl). Regarding Chl uncertainties, relations among MODIS, GOCI, and *in situ* Chl are extensively reported. Chl derived from MODIS and GOCI are significantly correlated and GOCI Chl estimates favorably agree with the *in situ* Chl in Tachibana Bay (Sakuno et al., 2013). In addition, Lamquin et al. (2012) reported that, although GOCI compares reasonably well with MERIS and MODIS, the current GOCI atmospheric correction systematically masks out data over very turbid waters. Thus, the higher RMSE with GOCI Chl when compared to NN-predicted Chl is due to the different algorithm for Case II waters from that for MODIS. Note that since the NN processes are trained with MODIS Chl, the RMSE is smaller than that for GOCI. Thus, the developed NN algorithm enables us to obtain Chl concentration even in cloudy regions with the level of a trained NN dataset.

Although we cannot predict Chl along coastal regions because of limited microwave capabilities as inputs, Chl predictability based on the NN algorithm can be applied to all other weather conditions. During the three NN processes (training, validation, and testing), we compute correlations and RMSEs to compare results with actual Chl values. However, when we apply the new inputs to a well-trained NN (Fig. 4), the RMSE between predicted and actual Chl may be different due to various input combinations (Figs. 5-8), as shown with Table 1. To reduce the RMSE between trained Chl and predicted Chl, we should use more input combinations. As long as the inputs are within the same ranges as those used for NN training, the NN can predict Chl with small uncertainties as discussed above. Therefore, challenges to a detailed understanding of the regional dynamics of both physics and biological activities remain and more research is needed to validate whether our approach is applicable to other seasons or regions.

This study seeks the feasibilities of filling the gaps using this NN algorithm rather than focusing on the scientific problems. However, our results suggest that the NN algorithm is a very promising approach for filling gaps due to clouds, high atmospheric water vapor, or even a typhoon passage, allowing investigation of many oceanographic phenomena using continuous Chl information. However, the Chl concentration close to coastal regions cannot be predicted due to the passive microwave's coverage, which is not applicable in near-coastal regions. This limitation can be overcome by additional NN processes using different inputs to fill gaps along coastal regions. SST is inversely related to Chl along coastal regions, and merged level 4 SST measurements (based on multiple satellite measurements) may be used for a major input in NN processes due to the better spatial coverage. If we combine the microwave-based Chl and level 4 SST data as separate inputs, we can obtain more complete Chl information.

ACKNOWLEDGEMENTS

This research was supported by the National Research Foun-

dation of Korea (NRF) grant funded by the Korean government (MSIP) (NRF-2014R1A2A1A11051742) and by the "Development of the integrated data processing system for GOCI-II" funded by the Ministry of Oceans and Fisheries, Korea.

REFERENCES

Ackerman, S. A., K. I. Strabala, W. P. Menzel, R. A. Frey, C. C. Moeller and L. E. Gumley (1998). Discriminating clear sky from clouds with MODIS, J. Geophys 103, 32141-32157.

Alvera-Azca´rate A., A. Barth, J. M. Beckers and R. H. Weisberg (2007). Multivariate reconstruction of missing data in sea surface temperature, chlorophyll, and wind satellite fields. J. Geophys Res 112(C3). doi: 10.1029/2006JC003660.

Alvera-Azcárate A., A. Barth, M. Rixen and J. M. Beckers (2005). Reconstruction of incomplete oceanographic data sets using empirical orthogonal functions: Application to the Adriatic Sea. Ocean Modell 9:325-346. doi: 10.1016/j.ocemod.2004.08.001.

Babin S. M., J. A. Carton, T. D. Dickey and J. D. Wiggert (2004). Satellite evidence of hurricane-induced phytoplankton blooms in an oceanic desert. J. Geophys Res 109(C3). doi:10.1029/2003JC001938.

Beckers, J. M. and M. Rixen (2003). EOF calculations and data filling from incomplete oceanographic data sets. J. Atmos Oceanic Technol 20(12), 1839-1856. doi: 10.1175/1520-0426(2003)020<1839:ECADFF>2.0.CO;2.

Buckton, D., E. O'Mongain and S. Danaher (1999). The use of neural networks for the estimation of oceanic constituents based on the MERIS instrument. International Journal Remote Sensing 20(9), 1841-1851.

Dzwonkowski, B. and X.-H. Yan (2005). Development and Application of a Neural Network based Ocean Color Algorithm in Coastal Water, International Journal of Remote Sensing 26(6): 1175-1200.

Eppley, R. W. (1972). Temperature and phytoplankton growth in the sea, Fishery Bulletin 70, 1068-1085.

Gross, L., S. Thiria, R. Frouin and B. G. Mitchell (2000). Artificial neural networks for modelling the transfer function between marine reflectance and phytoplankton pigment concentration. Journal of Geophysical Research 105(C2), 3483-3495.

Gross, L., S. Thiria and R. Frouin (1999). Applying artificial neural network methodology to ocean color remote sensing. Ecological Modeling 120, 237-246. doi: 10.1016/S0304-3800(99)00105-2.

IOCCG (2000). Remote Sensing of Ocean Colour in Coastal, and Other Optically-Complex, Waters. Sathyendranath, S. (ed.), Reports of the International Ocean-Colour Coordinating Group, No. 3, IOCCG, Dartmouth, Canada.

Jo, Y. H., M. Dai, W. Zhai, X. H. Yan and S. Shang (2012). On the variations of sea surface pCO_2 in the northern South China Sea: A remote sensing based neural network approach. J. Geophys Res 117(C8). doi: 10.1029/2011JC007745.

Kavak M. T. and S. Karadogan (2012). The relationship between sea surface temperature and chlorophyll concentration of phytoplanktons in the Black Sea using remote sensing techniques. J Environ Biol 33,493-8.

Keiner, L. and X.-H. Yan (1998). A neural network model for estimating sea surface chlorophyll and sediments from Thematic Mapper Imagery, Remote Sensing of Environment 66(2), 153-165.

Kim, T. W., R. G. Najjar and K. Lee (2014). Influence of precipitation events on phytoplankton biomass in coastal waters of the eastern United States, Global Biogeochem. Cycles 28, 1-13. doi: 10.1002/2013GB004712.

Kim, H.-C., S. Yoo and I. S. Oh (2007). Relationship between phytoplankton bloom and wind stress in the sub-polar frontal area of the Japan/East Sea, Journal of Marine Systems 67, 205-216.

Kondrashov D. and M. Ghil (2006). Spatio-temporal filling of missing data in geophysical data sets. Nonlinear Processes Geophys 13(2), 151-159. doi: 10.5194/npg-13-151-2006.

Lalli Carol M. and T. R. Parsons (1997). Biological Oceanography an Introduction (second edition), Open University, Elsevier, 337.

Lamquin, N., C. Mazeran, D. Doxaran, J.-H. Ryu and Y.-J. Park (2012). Assessment of GOCI radiometric products using MERIS, MODIS and field measurements, Ocean Sci. J. 47: 287. doi: 10.1007/s12601-012-0029-z.

Li, J., C. Y. Liu, H. L. Huang, T. J. Schmit, X. Wu, W. P. Menzel and J. J. Gurka (2005). Optimal cloud-clearing for AIRS radiances using MODIS, 1266 IEEE Transactions on Geoscience and remote sensing 43, 1266-1278. doi: 10.1109/TGRS.2005.847795.

Lin I. I., C. C. Wu, I. F. Pun and D. S. Ko (2008). Upper ocean thermal structure and the western North Pacific Category 5 typhoons. Part I: Ocean features and category-5 typhoon's intensification. Mon Weather Rev 136:3288-3306. doi: 10.5670/oceanog.2011.91.

Lin, I. I., W. T. Liu, C. Wu, G. T. F. Wong, C. Hu, Z. Chen, W. Liang, Y. Yang and K. Liu (2003). New evidence for enhanced ocean primary production triggered by tropical cyclone, Geophys. Res. Lett. 30(13), 1718. doi: 10.1029/2003GL017141.

Liu, C. Y., G. R. Liu, T. U. Lin, C. C. Liu, H. Ren and C. C. Young (2014). Using surface stations to improve sounding retrievals from hyperspectral infrared instruments, IEEE Transactions on Geoscience and Remote Sensing 52, doi: 10.1109/TGRS.2014.2305992.

Liu, Y., J. R. Key, R. A. Frey, S. A. Ackerman and W. P. Menzel (2004). Nighttime polar cloud detection with MODIS, Remote Sens. Environ. 92, 181-194.

Price J. F., T. B. Sanford and G. Z. Forristall (1994). Forced stage response to a moving hurricane. J. Phys Oceanogr 24, 233-260. doi: 10.1175/1520-0485(1994)024<0233:FSRTAM>2.0.CO;2.

Sakuno, Y., K. Makio, M. Koike and S. Kitahara (2013). Chlorophyll-a Estimation in Tachibana Bay by Data Fusion of GOCI and MODIS Using Linear Combination Index Algorithm, Advances in Remote Sensing 2, 292-296. doi: 10.4236/ars.2013.24032.

Schiller, H. and R. Doerffer (1999). Neural network for emulation of an inverse model-Operational derivation of Case II water properties from MERIS data. International Journal of Remote Sensing 20(9), 1735-1746.

Sirjacobs, D., A. Alvera-Azcárate, A. Barth, G. Lacroix, Y. Park, B. Nechad, K. Ruddick and J. M. Beckers (2011). Cloud filling of ocean colour and sea surface temperature remote sensing products over the southern north sea by the data interpolating empirical orthogonal function methodology. Journal of Sea Research 65(1), 114-130.

Siswanto E., J. Ishizaka, A. Morimoto, K. Tanaka, K. Okamura, A. Kristijono and T. Saino (2008). Ocean physical and biogeochemical responses to the passage of Typhoon Meari in the East China Sea observed from Argo float and multiplatform satellites. Geophys Res Lett 35(15). doi: 10.1029/2008GL035040.

Wang, P., J. Li, J. Li, Z. Li, T. J. Schmit and W. Bai (2014). Advanced infrared sounder subpixel cloud detection with imagers and its impact on radiance assimilation in NWP, Geophysical Research Letters 41. doi: 10.1002/2013/GL059067.

Zhang T., F. Fell, Z. S. Liu, R. Preusker, J. Fischer and M. X. He (2003). Evaluating the performance of artificial neural network techniques for pigment retrieval from ocean color in Case I waters. J Geophys Res 108(C9). doi: 10.1029/2002JC001638, 2003.

Zhao, H., D. L. Tang and Y. Wang (2008). Comparison of phytoplankton blooms triggered by two typhoons with different intensities and translation speeds in the South China Sea, Mar. Ecol. Prog. Ser. 365, 57-65. doi: 10.3354/meps07488.

Zheng G. M. and D. L. Tang (2007). Offshore and nearshore chlorophyll increases induced by typhoon winds and subsequent terrestrial rainwater runoff. Mar Ecol Prog Ser 333, 61-74. doi: 10.3354/meps333061.

Zheng Z. W., C. R. Ho and N. J. Kuo (2008). The importance of pre-existing oceanic conditions to upper ocean response induced by Super Typhoon Hai-Tang. Geophys Res Lett 35(20). doi: 10.1029/2008GL035524.